J Polym Res (2015) 22: 117
DOI 10.1007/s10965-015-0763-x

ORIGINAL PAPER

Effect of processing history on the rheological properties, crystallization and foamability of branched polypropylene

Yiwei Luo[1] · Chunling Xin[1,2] · Dalong Zheng[1] · Zhijiang Li[1] · Weilin Zhu[1] · Shenkang Wu[1] · Qitao Zheng[1] · Yadong He[1,2]

Received: 3 January 2015 / Accepted: 18 May 2015 / Published online: 26 May 2015

Abstract The effects of processing history and post-processing annealing procedure on the rheological properties of long-chain branched polypropylene (LCB-PP) have been studied intensively. It is found that melt flow index, swelling ratio, storage modulus and complex viscosity at low frequency, as measures of melt viscoelasticity for LCB-PP, were greatly influenced even by the short-time processing in an internal mixer. Further, the relationship between the magnitude of shear modification and total shear strain was linear on a logarithmic scale. Moreover, the rheological properties of processed LCB-PP were recovered by vacuum-annealing to some extent. It also demonstrates that more intense processing history resulted in longer time required for the recovery of rheological properties. As far as the recovery process was concerned, high-pressure CO_2 saturation annealing was much more effective than vacuum-annealing and more sufficient recovery was brought by higher saturation pressure. This superiority of high-pressure CO_2 saturation annealing was attributed to the larger free volume for PP chain movement, which shorten the annealing time required for long branches to recover to their initial states. Besides, the peak temperature during the crystallization of LCB-PP was substantially improved after processing. Meanwhile, the foamability of LCB-PP was deteriorated after shearing process, which manifested as larger cell size and lower cell density.

✉ Chunling Xin
xincl@mail.buct.edu.cn

✉ Yadong He
heyd@mail.buct.edu.cn

[1] College of Mechanical and Electrical Engineering, Beijing University of Chemical Technology, Beijing 100029, China

[2] Engineering Research Center for Polymer Processing Equipment, Ministry of Education, Beijing 100029, China

Keywords Branched polypropylene · Processing history · Rheological property · Recovery · Crystallization · Foaming behavior

Introduction

Microcellular plastics are widely used in insulation, packing, cushion, filters and other fields [1]. Polypropylene (PP) foam has many desired and beneficial properties, such as high melting point, high tensile modulus, excellent chemical resistance and recyclability. These properties make PP foam promising. However, there are still some problems for PP foaming. One of the biggest problems is the lack of melt elasticity, which is ascribed to the linear structure of molecules. Therefore, considerable effort has been carried out to enhance the melt elasticity of PP. The modification technique by peroxide and/or radiation has solved this problem very well, and expands the applications of PP [2–4]. This so-called high-melt-strength (HMS) PP shows good processability for various processing operations because of the enhanced strain-hardening in elongational viscosity. The origin of the marked strain-hardening is considered to be long-chain branches, and few papers have characterized the branch structure [3, 5].

It is well known that rheological properties of polymers strongly depend on the processing history the melt has undergone before [6, 7]. This is evident for branched polymers because the entanglement structure of the molecules was changed by shear deformation. Consequently, the viscosity and elasticity of branched polymer were reduced. This effect is called ‘shear modification’.

The role of long-chain branches on the rheological properties and thus processability has been studied extensively on low-density polyethylene (LDPE) for a long time. Rokudai et al. [8–10] have studied the effect of shear history on the

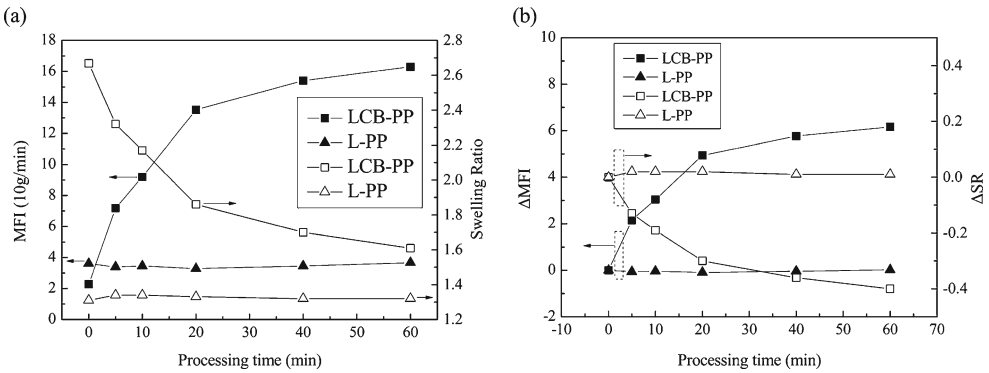

Fig. 1 MFI (closed symbol) and SR (open symbol) as a function of processing time for LCB-PP (square) and L-PP (triangle) processed at 40 rpm before (**a**) and after (**b**) normalization

rheological properties and processability of LDPE, and found that swelling ratio decreased with increasing processing time and/or temperature. Therefore, the quantitative analysis of the effect of processing history on the swelling ratio gave the information on the characterization of long-chain branches in LDPE. Yamaguchi et al. [11, 12] reported that intense processing history—high strain rate and/or long residence time in a processing machine—depressed the drawdown force notably. They also compared the rheological properties for LDPE processed by various kinds of conventional processing machines, i.e., a two-roll mill, an internal batch mixer and a co-rotating twin-screw extruder (Co-TSE). The results showed that the drawdown force would not be depressed by the intermittent stress history in a two-roll mill. Furthermore, it was also found that screw configuration in the Co-TSE affected the rheological properties to different degrees. Processing with conveying screws depressed the drawdown force more than that with kneading blocks as long as the torque and the residence time were the same [6]. However, the shear modification is reversible and the rheological properties can be recovered by solvent or annealing [8, 9, 12]. The origin of shear modification has been believed to be a disentanglement mechanism for a long time [13–15], but this idea was confuted by Leblans and Bastiaansen [16]. They found out that reduced interpenetration of the molecules cannot be the reason for the lower elongational viscosity. Thus they support the idea of alignment of side chains along the backbone as the origin of shear modification.

Because of the effect on the processability as demonstrated, shear modification behavior has to be comprehended when employing a branched polymer. As for the influence of shear treatment on long-chain branched PP (LCB-PP), only scant information is available. Yamaguchi et al. [6] compared LDPE, linear polypropylene (L-PP) and LCB-PP after processing in an internal batch mixer. They found that the drawdown force was strongly depressed even by the short processing time, whereas the rheological properties of L-PP were unchanged by the processing history. LCB-PP needed a longer post-processing annealing time to recover the drawdown force than LDPE. Breuer et al. [17] investigated the shear modification recovery, and demonstrated that the rate of recovery strongly depended on the degree of LCB. However, there is seldom research on shear modification of LCB-PP, and the characterization of rheological properties of shear modified LCB-PP is not comprehensive. Besides, the protective medium is limited to low-pressure nitrogen on the previous literatures about the effect of annealing on the recovery of rheological property, and no one investigates the type of protective medium and annealing parameters.

In addition, many literatures have focused on the crystallization [18–24] and foaming behavior [25–27] of LCB-PP, and some researchers have studied the impact of shear on the crystallization of high density polyethylene [28] and poly (ethylene-co-octene) [29]. However, to the best of our knowledge, there is little research on the effect of processing history on the crystallization and foamability of LCB-PP. In this study, we have clarified the effect of processing history on the

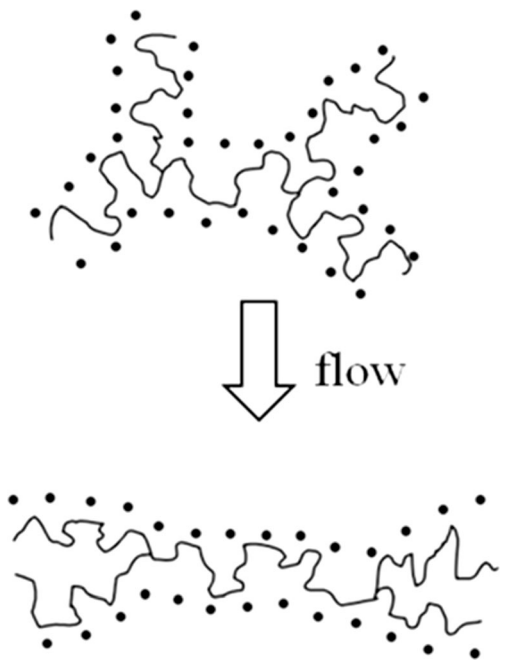

Fig. 2 Schematic illustration of molecular conformation before and after shear modification, based on the tube model

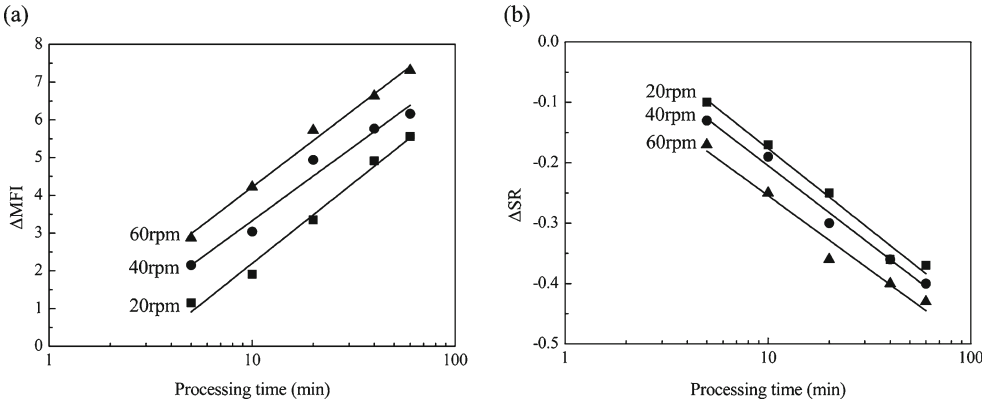

Fig. 3 Effects of rotor speed and processing time on extent of shear modification for LCB-PP: square for 20 rpm, circle for 40 rpm and triangle for 60 rpm

rheological properties, crystallization and foamability of LCB-PP. The recovery of rheological properties under different protective media and annealing procedures was also studied in detail.

Experimental

Materials

Polymers used in this study included LCB-PP [Borealis, Daploy WB140HMS, melt flow index (MFI)=2.3 g/10 min at 230 °C, 2.16 kg], and L-PP (Sinopec Yangzi Petrochemical Co. Ltd., China, T03-H, MFI=3.6 g/10 min at 230 °C, 2.16 kg). Carbon dioxide (CO_2) (purity 99 %) was purchased from Oxygen Plant, Beijing, China.

The number- and weight-average molecular weights of LCB-PP, measured by gel permeation chromatography (GPC), are $M_n=6.6\times10^4$, $M_w=4.3\times10^5$, and $M_w/M_n=6.5$, respectively; those of L-PP are as follows: $M_n=5.9\times10^4$, $M_w=4.5\times10^5$, and $M_w/M_n=7.6$. Nuclear magnetic resonance (NMR) measurements also revealed that the number of long (≥C6) branches for LCB-PP is less than 1 per 1000 carbon atoms.

Processing history

The processing histories of LCB-PP and L-PP were applied by an internal batch mixer (HAAKE, Polylab) at 190 °C for various processing times with a small amount of thermal stabilizer. The rotor speed for LCB-PP was changed from 20 to 60 rpm (the average shear rate was about 3.6 to 10.9 s^{-1}), and that for L-PP was 40 rpm (the average shear rate was about 7.3 s^{-1}). A part of processed samples were plunged into an ice-water bath to freeze the macroscopic molecular motion; another part of processed LCB-PPs were immediately compressed into 1-mm-thick sheets by a compression-molding machine for 3 min at 190 °C. Original pellets of LCB-PP were also compressed into a sheet form. These sheets would be used in dynamic rheological measurement and foaming experiment.

Annealing

The annealing procedure of processed LCB-PP was applied by a vacuum drying oven (Shanghai Linpin Instrument Stock Co. Ltd., DZF-6050) at different temperatures for various residence times; this annealing procedure was named as

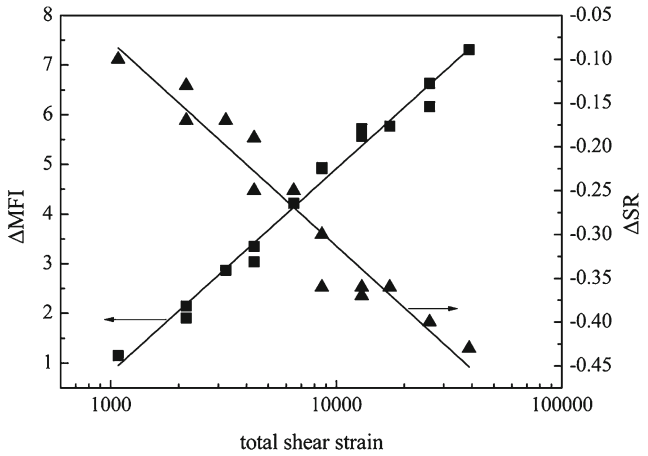

Fig. 4 Linear correlation between ΔMFI/ΔSR and log total shear strain for LCB-PP

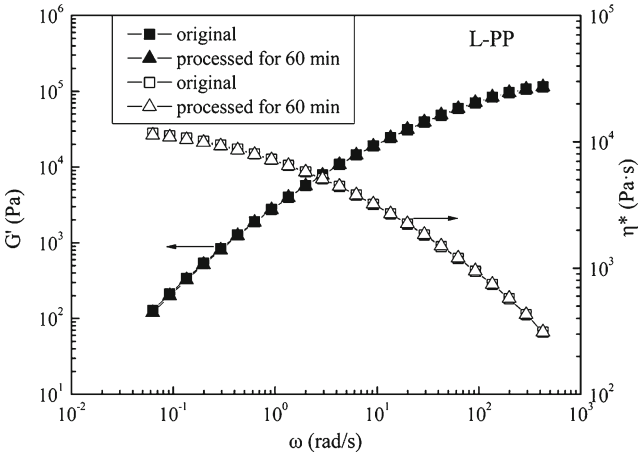

Fig. 5 G' and η^* of L-PP processed by internal mixer at 40 rpm and 190 °C for 60 min

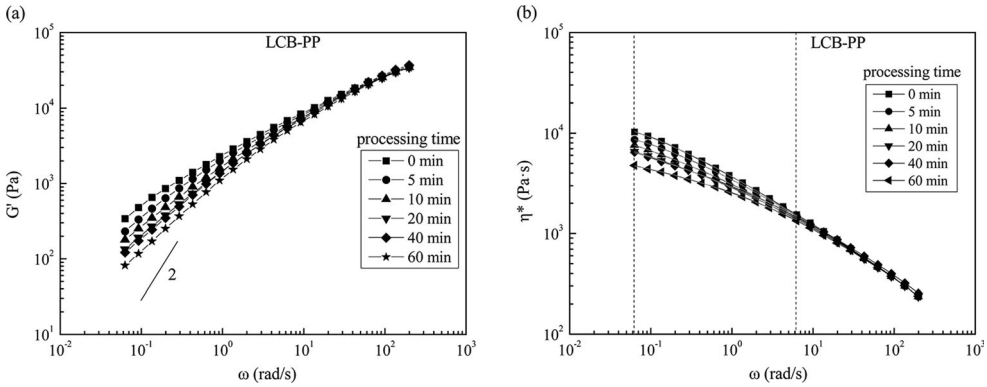

Fig. 6 G' and η^* of LCB-PPs processed by internal mixer at 40 rpm and 190 °C with various processing times

'vacuum-annealing'. Meanwhile, another annealing procedure, named as 'high-pressure CO_2 saturation annealing', was performed by a self-developed high-pressure vessel at 200 °C but different CO_2 pressures for 240 min. In order to prevent the annealed samples from foaming, the vessel was quickly cooled down to 80 °C within 20 min before the removal of samples.

Batch foaming

The LCB-PP sheets with different processing histories were enclosed in a high-pressure vessel preheated to 50 °C. The vessel was flushed with low pressure CO_2 for 2 min, followed by increasing the pressure to 20 MPa and maintained for 10 h to ensure equilibrium adsorption for CO_2. Then, the samples were removed out after a rapid quench of pressure and transferred within a 2 min interval to a silicone oil bath kept at 190 °C for different times, then quenched in cold water.

Characterization

MFIs of PPs were measured on an MFI tester (MTS Industrial Systems Co. Ltd., ZRZ1452) at 230 °C with an applied load of 2.16 kg. Swelling ratio (SR) was taken as the ratio of the diameter of the cold extrudate to the diameter of the die. The final MFI of each sample was taken as the mean of three tests of MFI, so was the final SR.

Table 1 Rheological parameters of processed LCB-PPs

Processing time (min)	η_0 (Pa·s)	λ (s)	n	Terminal slope of G'
0	11618	19.4	0.56	0.73
5	9522	17.9	0.60	0.83
10	8769	15.4	0.63	0.84
20	7460	13.8	0.66	0.89
40	7379	13.0	0.68	0.92
60	4973	11.4	0.71	0.98

The changes in MFI and SR on shear modification were normalized respectively, and expressed as:

$$\Delta \mathrm{MFI} = \frac{\text{Final MFI-Original MFI}}{\text{Original MFI}} \quad (1)$$

$$\Delta \mathrm{SR} = \frac{\text{Final SR-Original SR}}{\text{Original SR}} \quad (2)$$

A rotational rheometer (HAAKE, MARS III), with a parallel-plate geometry (diameter is 20 mm), was used for dynamic rheological measurements. Small amplitude oscillatory shear was performed in the frequency range 0.01-100 Hz at 200 °C. A strain of 0.5 % was used, which was in the linear viscoelastic regime for all samples.

The crystalline behavior of processed LCB-PP was studied on a differential scanning calorimeter (DSC) (TA Instruments, Q20). The measurements were performed in nitrogen atmosphere as following procedures: samples were heated to 200 °C at 80 °C/min and kept for 3 min to erase any previous thermal history, then cooled to 60 °C at 10 °C/min to determine the temperature at the peak of the exothermic curve. The

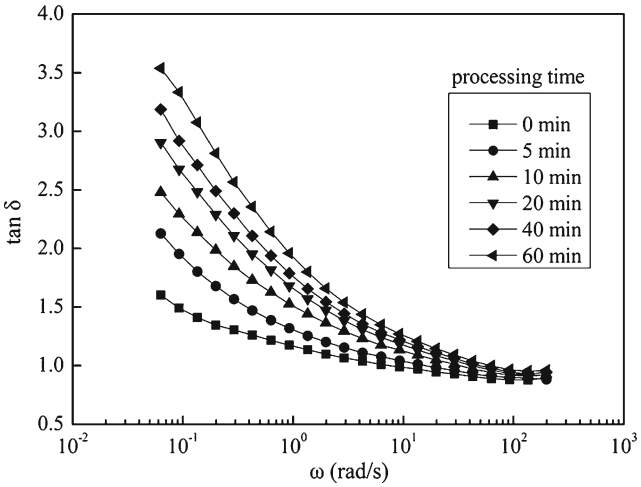

Fig. 7 Tanδ of LCB-PPs processed by internal mixer at 40 rpm and 190 °C with various processing times

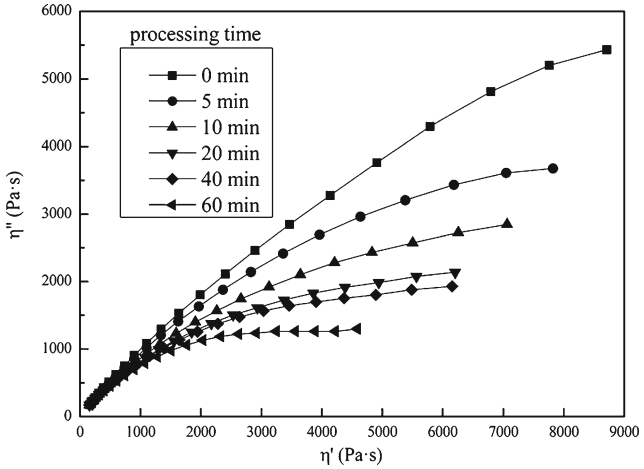

Fig. 8 Cole-Cole plot of LCB-PPs processed by internal mixer at 40 rpm and 190 °C with various processing times

melting points and crystallinities of LCB-PPs used for foaming were also measured as follows: samples were heated to 200 °C at 10 °C/min to determine the endothermic curve. The crystallinity, X_c, was estimated by using the relation $X_c = -\Delta H_m/\Delta H_{m0}$, where ΔH_m was the melting enthalpy per gram of a sample and ΔH_{m0} was that of 100 % crystalline PP with a constant of 209 J/g [30].

The cell morphologies of LCB-PP foams were characterized by a scanning electron microscope (SEM) (Hitachi, S4700). The foams were immersed in liquid nitrogen for 5 min and then fractured. The fractured surfaces with Pt-Pd coating were scanned with SEM. The average cell size was computed via analysis of SEM photographs on ImageJ software. The number average diameter of all cells in one micrograph, $\bar{d}$, was calculated as follows:

$$\bar{d} = \frac{\sum_{i=1}^{n} d_i}{n} \tag{3}$$

where d_i is the diameter of a single cell, and n is the number of counted cells. At least 100 cells were selected randomly from the SEM graph of each sample to evaluate the average diameter.

The volume expansion ratio of the foamed sample, R_v, was defined as the ratio of the bulk density of the unfoamed one (ρ_0) to that of the foamed one (ρ_f):

$$R_v = \frac{\rho_0}{\rho_f} \tag{4}$$

ρ_0 and ρ_f were measured via water displacement method according to ASTM D792-00.

Void fraction of the foamed sample, v_f, was defined as the ratio of the volume of gas (v_g) to that of the foam (v_g+v_p):

$$v_f = \frac{v_g}{v_g + v_p} \tag{5}$$

The cell density N_0, defined as the number of cells per unit volume of the polymer, was determined as follows:

$$N_0 = \left[\frac{nM^2}{A}\right]^{3/2} R_v \tag{6}$$

where A is the area of an SEM graph (cm^2), n is the number of cells in the micrograph, M is the magnification factor, and R_v is the expansion ratio.

Results and discussion

Changes in MFI and SR resulting from shearing

MFI, which is an important index of the melt flowability in polymer processing, is mainly a measure of melt viscosity; while SR is a very good indication of melt elasticity for polymers and is very sensitive to the viscoelastic variation caused by the shear processing. Therefore, the rheological properties of the melt were characterized by MFI and SR in this paper. In Fig. 1, the MFI and SR of LCB-PP were greatly affected by shearing, and the ΔMFI increased to 2 even under short processing time (5 min). The curves of ΔMFI and ΔSR became gentle when the processing time exceeded 20 min. However,

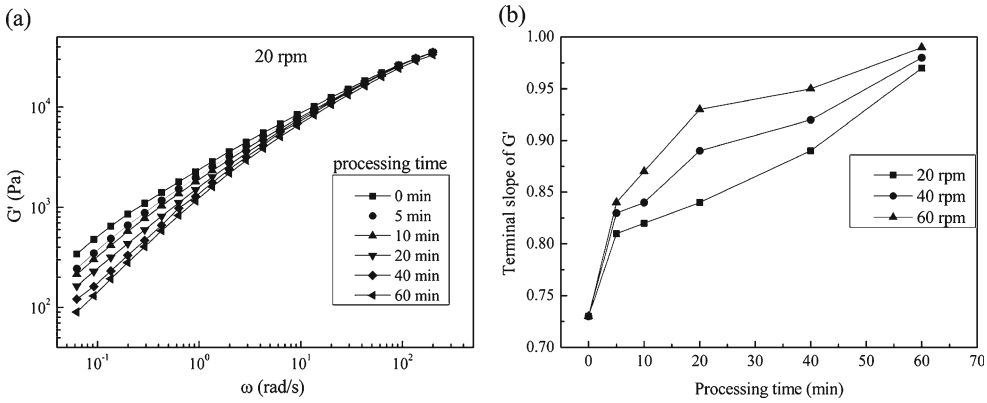

Fig. 9 Effect of shear history on the rheological properties of LCB-PP: (**a**) *G'* (**b**) terminal slope of *G'*

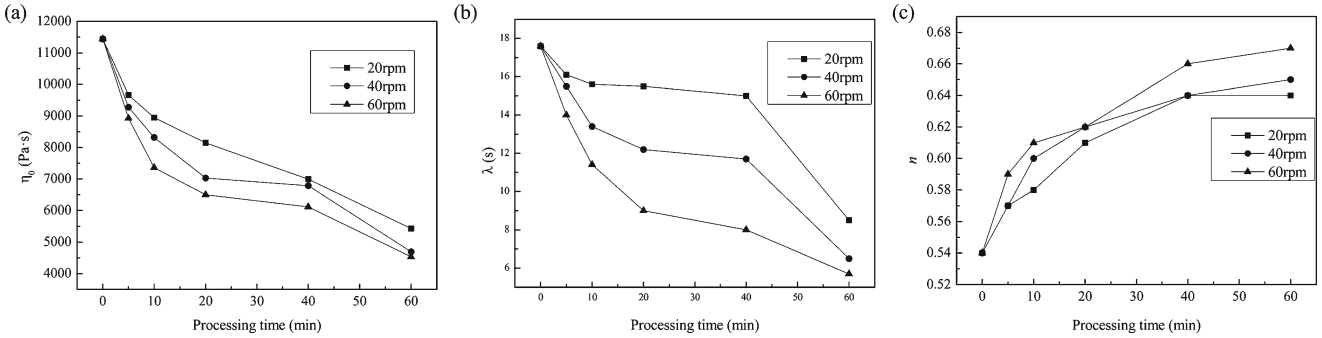

Fig. 10 Effect of shear history on the rheological parameters LCB-PP with various shear histories: (**a**) η_0, (**b**) λ and (**c**) n

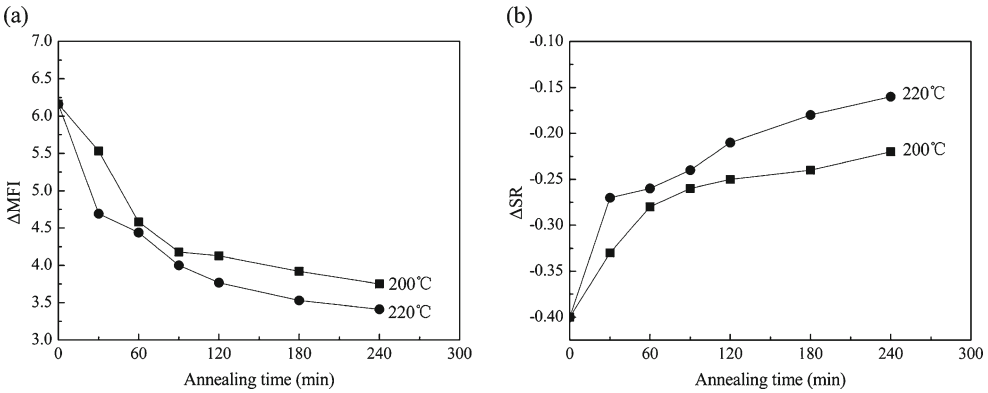

Fig. 11 Effects of varying vacuum-annealing times and annealing temperatures on the recovery of rheological properties for LCB-PP processed at 190 °C and 40 rpm for 60 min

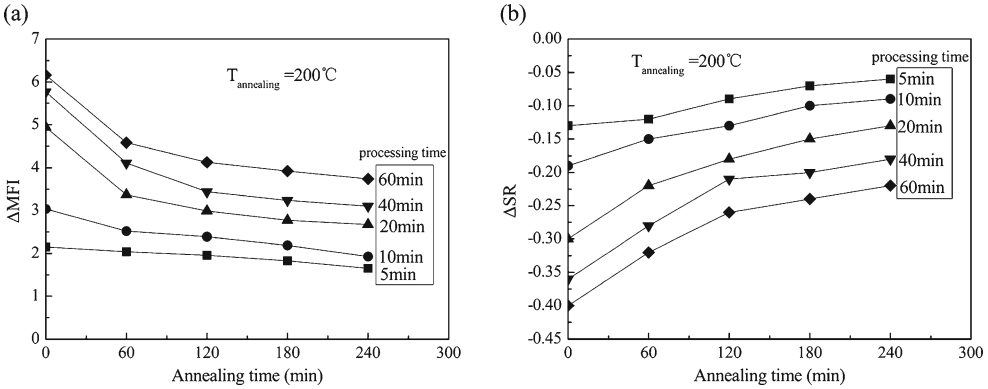

Fig. 12 Recovery curves of rheological properties after vacuum-annealing procedure for the LCB-PPs processed by the internal mixer at 190 °C and 40 rpm for various processing times: 5 min (square), 10 min (circle), 20 min (upper triangle), 40 min (lower triangle) and 60 min (diamond)

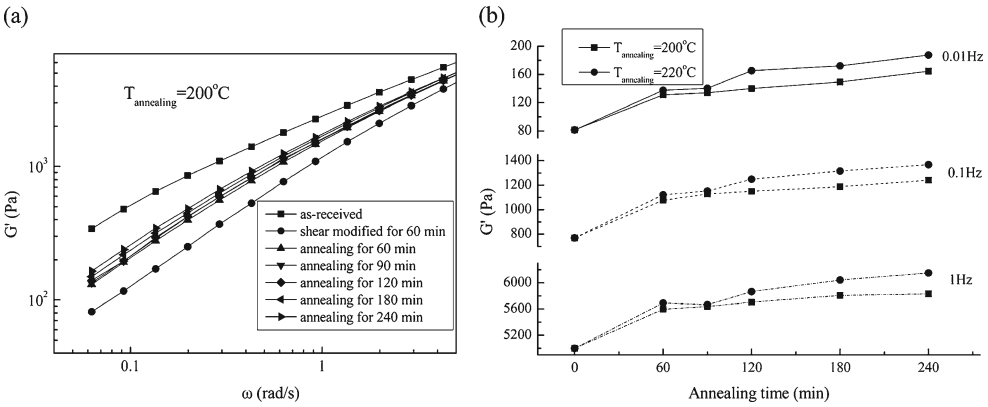

Fig. 13 *G'* of shear modified LCB-PPs after vacuum annealing at different temperatures

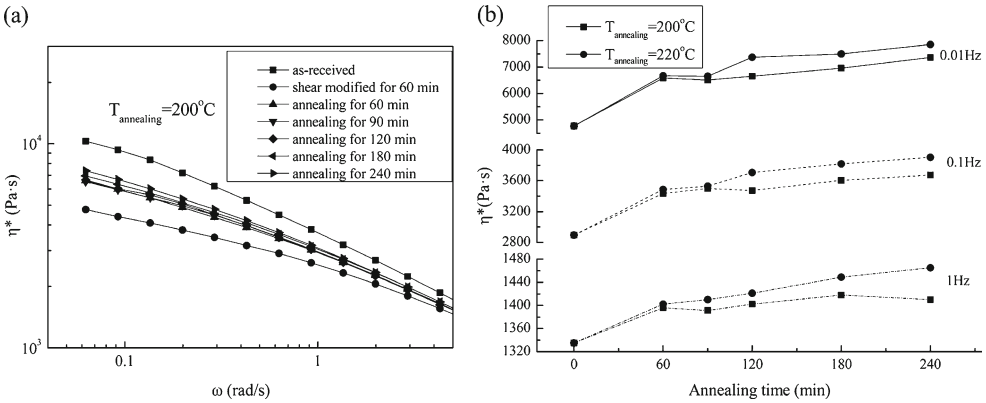

Fig. 14 η^* of shear modified LCB-PP after vacuum annealing at different temperatures

shearing had little effect on the rheological properties of L-PP, and the ΔMFI and ΔSR maintained near zero. The difference of molecular chain between LCB-PP and L-PP should be responsible for the difference of rheological properties. According to the Doi-Edwards theory [31], conformation change of long-chain branches had to take place by utilizing contour length fluctuation, or retraction to the branch point within the tube. Hence, the relaxation time of LCB-PP was very long, along with the low MFI and high SR. However, exposure to flow and deformation in a processing machine dragged the branches into the same tube of a backbone chain [16]. Consequently, contraction of backbone chains between branch points took place easily, as with a linear polymer, which resulted in the high MFI and low SR. The schematic model of molecular conformation, based on the tube model, is illustrated in Fig. 2, in which dots denote neighbor chains. In contrast, the rheological properties of L-PP would not be much affected by shearing due to its linear molecular conformation.

The effects of varying rotor speeds and processing times on the ΔMFI and ΔSR for LCB-PP are shown in Fig. 3. Plots of ΔMFI against processing time for three different rotor speeds are given in Fig.3a. The relationships are linear and the lines for different rotor speeds are almost parallel and equally spaced on a logarithmic scale. For ΔSR, the same relationships can be observed. As average shear rate in the batch mixer is proportional to rotor speed; therefore, it follows that the relationship between ΔMFI/ΔSR and log total shear strain (average shear rate×processing time) should also be linear. This is indeed so, as can be seen from the results in Fig. 4. It should be noted that the linear correlation between ΔMFI and total shear strain is superior to that between ΔSR and total shear strain, which is in accordance with the results obtained by Hanson [13]. This linear correlation between ΔMFI and total shear strain is fitted by the equation

$$\Delta MFI = 4.09 \times lg(total\ shear\ strain) - 11.47 \quad (7)$$

In Fig. 5, curves of G' and η^* for L-PP processed for 60 min coincide exactly with those of L-PP without processing, indicating that the rheological property of L-PP would not be affected by shear. But in Fig. 6a, the notable decrease of G' at low frequency with increasing processing time indicates the decrease of melt elasticity of LCB-PP. In the terminal zone, G' of linear polymers follow the well-known frequency dependence, i.e., terminal behavior [32]. However, LCB-PPs with different processing histories are deviated from the terminal behavior. With the increase of processing time, the terminal slope of G' increased from 0.73 of 0 min curve to 0.98 of 60 min curve. Because of the disentanglement and alignment of side chains along the backbone, the molecular chain of LCB-PP acted more like a linear chain after long processing, presented as the terminal slope much closer to 2 of linear polymer. Likewise, the obvious decrease of η^* at low frequency means the decrease of viscosity in Fig. 6b. The Newtonian-plateau at low frequency became evident and the shear-thinning became started at higher frequency with the prolonged processing time. The viscosity of the sample was fitted by the Carreau equation, and the parameters including zero-shear viscosity (η_0), relaxation time (λ) and shear-thinning index (n) are listed in Table 1. It can be seen that with the prolonged processing time, the rheological parameters changed regularly, i.e., η_0 and λ decreased and n increased gradually. These suggest a lower viscosity and weaker long

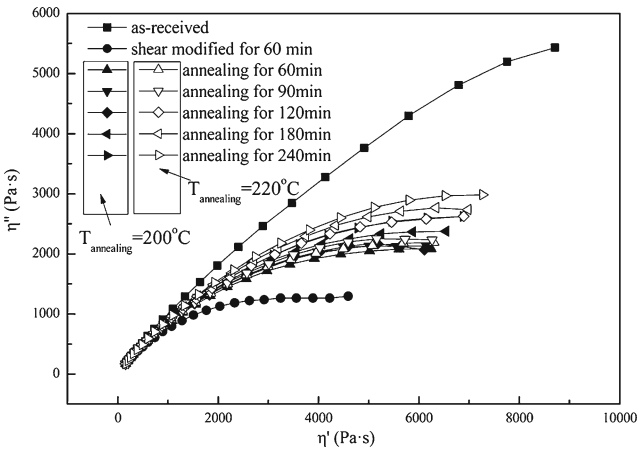

Fig. 15 Cole-Cole plot of shear modified LCB-PP after vacuum annealing at different temperatures

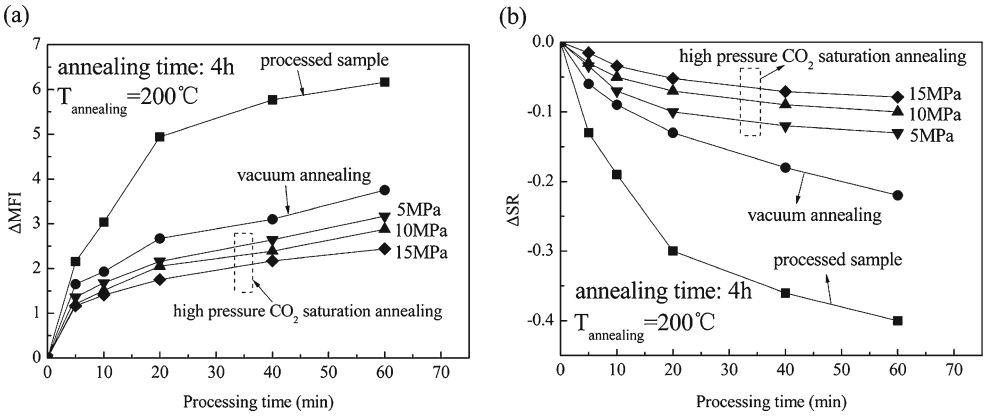

Fig. 16 Recovery curves of rheological properties during different annealing procedures for the samples processed by the internal mixer for various processing times at 190 °C and 40 rpm

relaxation mechanism and shear-thinning resulted from the change of molecular conformation.

It has been shown that the loss angle (δ) is independent of the frequency in a limited frequency range since polymers with LCB have the gel-like rheological behavior. Moreover, with LCB level increasing, the plateau of δ becomes more evident and the value of δ decreases [33]. In Fig.7, with the increase of processing time, tan δ increased continually at low frequency and the plateau became shorter. For the 60 min curve, tan δ ascended with the frequency decreasing, which is a typical terminal behavior of liquid-like material.

The non-terminal behavior of LCB-PP can also be illustrated in Cole-Cole plot [34]. The radius of semicircle gradually decreased with increasing processing time in Fig. 8, demonstrating that the branched PP began to act like linear chain after suffering from shear. The Cole-Cole plot of the sample without processing showed evident upturning at high viscosity, indicating that a longer relaxation time appeared; while this phenomenon gradually became indistinct with the increasing processing time, indicating that the long relaxation mechanism disappeared gradually.

In Fig. 9a, G' of LCB-PP at low frequency declined obviously with prolonged processing time under the same rotor speed, suggesting the remarkable drop of melt elasticity. According to Fig. 9b, terminal slope of G' at low frequency increased with processing time and rotor speed. It means that longer processing history resulted in weaker non-terminal behavior and more like linear chain behavior. Similarly, the complex viscosity curves of LCB-PPs processed at different rotor speeds and processing times were fitted by Carreau model, and the relationship between η_0 and processing history was shown in Fig. 10, so was λ and n. Increasing both processing time and rotor speed resulted in depressed viscoelasticity and shear-thinning behavior.

Recovery of rheological properties of LCB-PP after post-procedure annealing

Because the alignment of side chains along the backbone during shearing process of LCB-PP is a physical process, this molecular orientation can be transformed into entangled structure by heat treatment. Figure 11 exemplifies the recovery curves of ΔMFI and ΔSR, i.e., the time variation of recovery process of melt elasticity for the LCB-PP processed at 190 °C and 40 rpm for 60 min. Lower ΔMFI and higher ΔSR were obtained with longer vacuum-annealing time, and they were gradually closer to the original value along with annealing time. Moreover, it is found that this recovery process was accelerated under higher annealing temperature. The recovery of rheological properties by exposure to annealing can be ascribed to the relaxation of molecular conformation from a low entropy state, especially around branch points, to the equilibrium state by micro-Brownian motion. Therefore, higher temperature enabled the rheological properties to recover more quickly.

Figure 12 displays the recovery of rheological properties of the processed LCB-PP after vacuum-annealing. The ΔMFI

Table 2 Rheological properties before and after annealing procedures for the samples processed for 60 min, as well as the recovery ratios of rheological properties after annealing

samples	ΔMFI	recovery ratio	ΔSR	recovery ratio
processed sample	6.16	–	–0.40	–
vacuum-annealing	3.75	39.1 %	–0.22	45.0 %
high-pressure CO_2 saturation annealing (5 MPa)	3.17	48.5 %	–0.13	67.5 %
high-pressure CO_2 saturation annealing (10 MPa)	2.88	53.2 %	–0.10	75.0 %
high-pressure CO_2 saturation annealing (15 MPa)	2.44	60.4 %	–0.079	80.3 %

Table 3 Solubility of CO_2 in branched PP

Temperature (°C)	Pressure (MPa)	Solubility (%) (SS $X_{corrected}$)
200	3.51	2.33
	7.02	4.81
	10.48	7.30
	13.96	9.82
	17.45	12.25

and ΔSR for all samples with different processing times seem to recover to the same, original value, suggesting that the number of long-chain branches and the molecular weight are unchanged. Therefore, the rheological modification by the applied processing history as well as the annealing procedure is not originated from the molecular scission and/or crosslink reaction, but from the conformation change of molecules as similar to the case of a low-density polyethylene. However, it took a longer time for LCB-PP to recover the rheological properties compared with LDPE. Moreover, more intense processing history resulted in longer annealing time required for the recovery of rheological properties. According to Yamaguchi [35], LCB-PP had less relatively 'short' long-branches than LDPE, resulting in the longer time of full recovery of rheological properties. In fact, the difference of molecular flexibility between polypropylene and polyethylene should be another important factor responsible for that slow recovery process. There are methyl groups on the backbone and branches of LCB-PP, making molecular chain of LCB-PP less flexible than that of LDPE. Thus, a higher energy barrier is needed to overcome for the recovery of molecular conformation of LCB-PP. Finally, a longer time was spent in the recovery of rheological properties of LCB-PP.

As shown in Fig. 13a, for the post-procedure annealing of LCB-PP processed at 40 rpm for 60 min, *G'* at low frequency gradually increased with the increasing annealing time at 200 °C, indicating that melt elasticity was recovered partially. It can be seen from Fig. 13b that *G'* at low frequency was improved when the annealing temperature was raised from 200 °C to 220 °C. Nevertheless, the *G'* of LCB-PP after annealing was still lower than that of as-received LCB-PP. This shows that very long annealing time should be spent in completely recovering the elasticity of shear modified samples.

At the same time, η^* at low frequency was greatly improved by annealing treatment in Fig. 14, and these curves were much steeper, presenting much more obvious shear-thinning behavior. The change of η^* demonstrates that the disentangled side chains recovered to their initial states by annealing, causing the improvement of viscosity. In addition, higher annealing temperature resulted in higher recovery strength of η^*.

In Fig. 15, the semicircle radius of Cole-Cole plot increased with annealing time, demonstrating that the aligned side chains were motivated in annealing to recover to entanglement state, and longer annealing time led to higher entanglement degree. Since micro-Brownian motion can be quicken by higher annealing temperature, then fierce molecular movement accelerated the recovery process of melt viscoelasticity. Therefore, the semicircle radius of the sample annealed at 220 °C is larger than that annealed at 200 °C with same annealing time in Fig. 15.

It is reported in literature [8] that the swelling of shear modified LDPE was completely recovered by solvent treatment, indicating that solvent treatment was more efficient than heat treatment. In this work, high-pressure CO_2 saturation annealing was used as a new annealing procedure for processed LCB-PP. The saturation pressure was 5 MPa, 10 MPa and 15 MPa, respectively. As shown in Fig. 16, the recovery strength of rheological properties after high-pressure CO_2 saturation annealing was much higher than that after vacuum-annealing. What is more, the stronger shear modification, the greater comparative advantage that high-pressure CO_2 saturation annealing showed in the recovery of rheological properties. The rheological properties of processed LCB-PPs before and after annealing are listed in Table 2. For the sample processed for 60 min, the recovery ratios of ΔMFI and ΔSR after vacuum-annealing are 39.1 % and 45.0 %, respectively; while

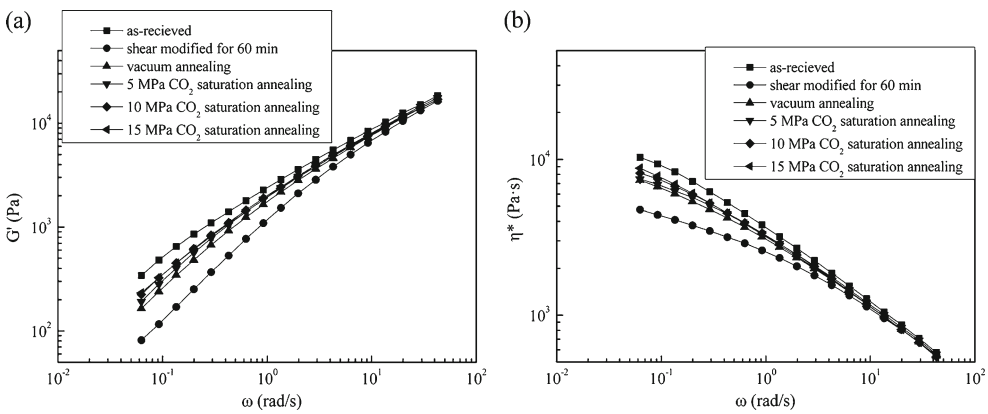

Fig. 17 *G'* and η^* of LCB-PPs before and after annealing treatments

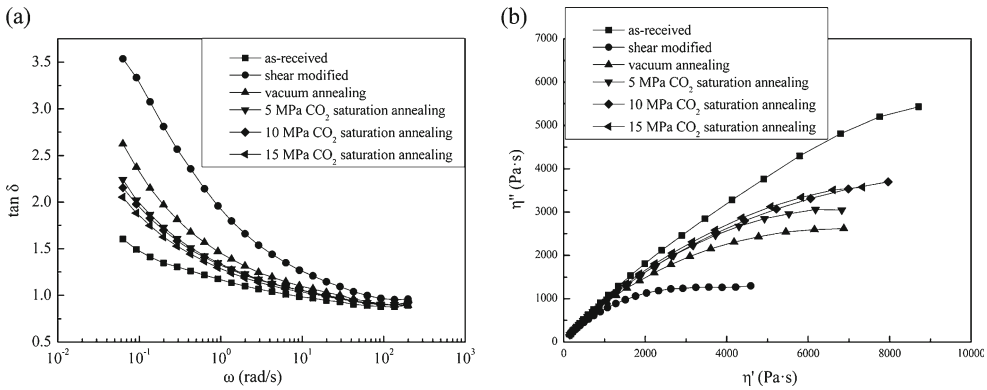

Fig. 18 Tan δ and Cole-Cole plot of LCB-PPs before and after annealing treatments

the results after high-pressure (5 MPa) CO_2 saturation annealing are 48.5 % and 67.5 %, respectively. We believe that the difference in free volume of PP between vacuum-annealing and high-pressure CO_2 saturation annealing resulted in the different recovery curves. Based on the lattice theory [36], the free volume of PP will be expanded when CO_2 molecules diffuse into. The activity ability of PP molecular chains will be enhanced due to the expansion of free volume. Therefore, it was much easier for aligned long-chains to recover to their initial states. This effect is presented as the higher recovery ratio after high-pressure CO_2 saturation annealing. The higher solubility of CO_2 in PP under higher saturation pressure (Table 3) [37] resulted in the larger free volume of PP and subsequent higher recovery ratio, as shown in Fig. 16 and Table 2.

Figure 17 shows the G' and η^* of LCB-PPs before and after different annealing processes. For the recovery process of viscoelasticity of LCB-PP processed for 60 min, high-pressure CO_2 saturation annealing was much more effective than vacuum annealing, and this superiority was presented as much higher G' and η^* at low frequency. The improvement of viscoelasticity was attributed to the quick entanglement of aligned side chains after the introduction of CO_2 molecules. Meanwhile, the higher solubility of CO_2 in PP, which was resulted from higher saturation pressure, further enhanced the molecular movement of PP. As a consequence, as Fig. 17 shows, both G' and η^* at low frequency gradually increased as saturation pressure of CO_2 increased.

As shown in Fig. 18a, tan δ of shear modified samples decreased quickly at low frequency and the curves started to flatten after annealing. In contrast, lower tan δ and gentler curve were obtained after high-pressure CO_2 saturation annealing. What's more, tan δ gradually decreased when the saturation pressure of CO_2 was increased. In Fig. 18b, the bigger semicircle radii of samples after annealing indicated a more obvious entanglement of side chains, and the bigger radius demonstrated that high-pressure CO_2 saturation annealing help the recovery of rheological property of sheared LCB-PP more than vacuum annealing. The fact that the radius of Cole-Cole plot increased with the rise of saturation pressure implied that increasing CO_2 saturation pressure is another method to quicken recovery of rheological property, excepting the longer annealing time.

Effect of processing history on non-isothermal crystallization of LCB-PP

Figure 19 shows the non-isothermal crystallization curves of as received LCB-PP and LCB-PP samples processed at 190 °C and 40 rpm for various processing times. The evident change in these exothermic curves suggested that processing history greatly influenced the non-isothermal crystallization behavior of LCB-PP. The exothermic peak (T_p) on DSC crystallization trace was raised from 127.4 °C to 129.4 °C after 5 min processing. This phenomenon would be ascribed to the branch structure. In other words, the difference of T_p involved in the information on the molecular shape. As discussed previously, side chains of LCB-PP aligned along the backbone during shearing process, making the chains move like linear ones. So it was much easier for these chains to fold back and forth repetitively and to form thin lamellae. Therefore, the T_p was evidently raised. With different processing times, the T_p of LCB-PP changed and moved to higher temperatures. If enough processing time was applied, the T_p could reach a potential maximum value at 129.9 °C and ranged from 129.2 to 129.9 °C. Figure 20 shows the dependence of the

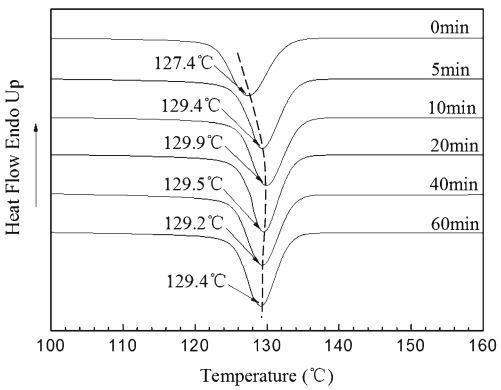

Fig. 19 Non-isothermal crystallization behavior of LCB-PPs processed at 190 °C and 40 rpm for various processing times

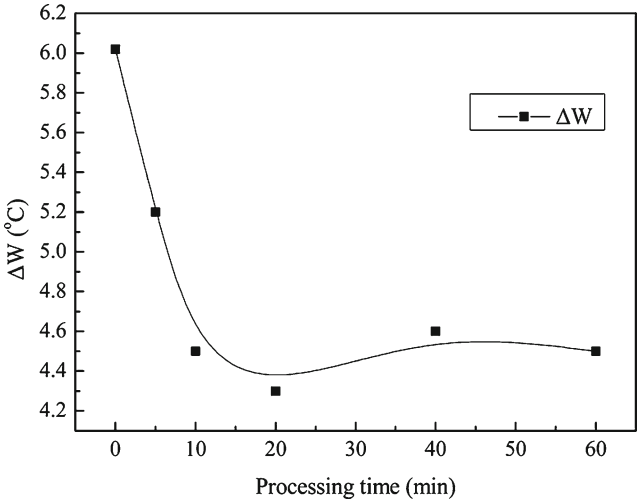

Fig. 20 Dependence of the width at half-height of the exotherm peak (ΔW) on processing time

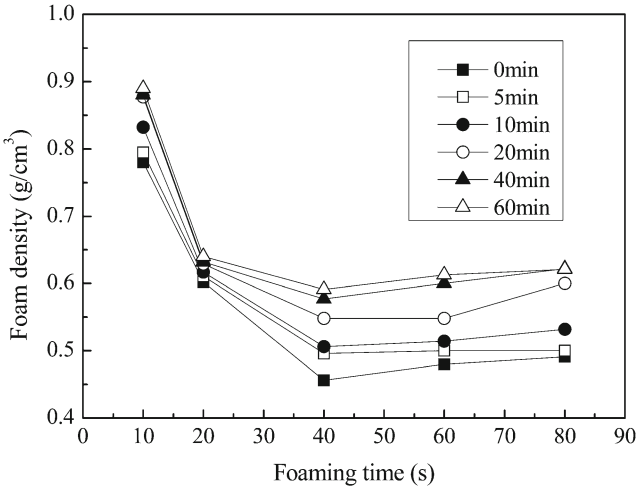

Fig. 21 Foam densities of LCB-PPs with various processing histories obtained by saturating at 50 °C and 20 MPa for 10 h, then foaming at 190 °C

width at half-height of the exothermic peak (ΔW) on processing time, and it can be seen that ΔW gradually decreased with the increasing processing time. In general, the smaller the ΔW, the faster the crystallization rate [38]. Hence, the crystallization rate of LCB-PP was increased by shear and the longer the processing time, the faster the crystal growth rate.

Effect of processing history on the foamability of LCB-PP

The melting points and crystallinities of unfoamed LCB-PPs with various processing histories are listed in Table 4. It is found that there is little difference among these LCB-PPs used for foaming in melting point and crystallinity. Because the absorption of CO_2 took place almost exclusively through the amorphous regions, it is believed that the solubility of CO_2 kept the same in these samples under the same condition. Figure 21 shows the foam densities of LCB-PPs with various processing histories obtained by saturating at 50 °C and 20 MPa for 10 h, and foaming at 190 °C. The foam density decreased quickly in the first stage and then increased slowly along with time. When the foaming time was 40 s, the foam densities of all samples reached their minimum values simultaneously, and their cell morphologies are shown in Fig. 22.

Table 4 Thermal properties of LCB-PPs with various processing times

Processing time (min)	Melting point (°C)	ΔH_m (J/g)	Crystallinity (%)
0	159.0	98.8	47.3
5	158.6	100.3	48.0
10	158.6	97.4	46.6
20	158.5	99.5	47.6
40	159.1	99.4	47.6
60	159.4	100.9	48.3

With the increase in processing time, the area of umfoamed regions in the LCB-PPs foams increased gradually, and the cell size distribution of LCB-PPs foams became non-uniform. With the increasing processing history applied on LCB-PP, the cell diameter increased initially then reduced, and the cell density decreased continuously in Fig. 23a. The change laws of cell diameter and cell density are also visually displayed in Fig. 22. The significant difference in cell morphology may be attributed to the difference in melt elasticity. As mentioned above, the melt elasticity of LCB-PP decreased with the increase of processing time. Cell coalescence took place during the cell growth when the foaming temperature was above the melting point of LCB-PP. This coalescence phenomenon became more evident with the decrease of melt elasticity; thus, the void fraction of foamed LCB-PP decreased when increasing the processing time, as shown in Fig. 23b. So, the cell diameter rose rapidly and the cell density declined gradually. At the same time, the bubble shrinkage happened due to the rapid escape of CO_2 from the bubbles at high temperature. Thus, no big-cells but several small-cells can be observed in Fig. 22f. Similar results have also been observed in the experiment of Zhai et al. [39]. Cell coalescence also resulted in the change of cell size distribution of foamed sample, as shown in Fig. 24. Outside the curve of 60 min, the cell diameter distribution became broader and the curves shifted to larger cell diameter along with the increase of processing time.

Conclusions

The effect of applied processing on the rheological properties, especially MFI, SR, G' and η^*, as measures of melt viscoelasticity, for LCB-PP has been studied as compared with those for L-PP. The viscoelasticity of LCB-PP was greatly

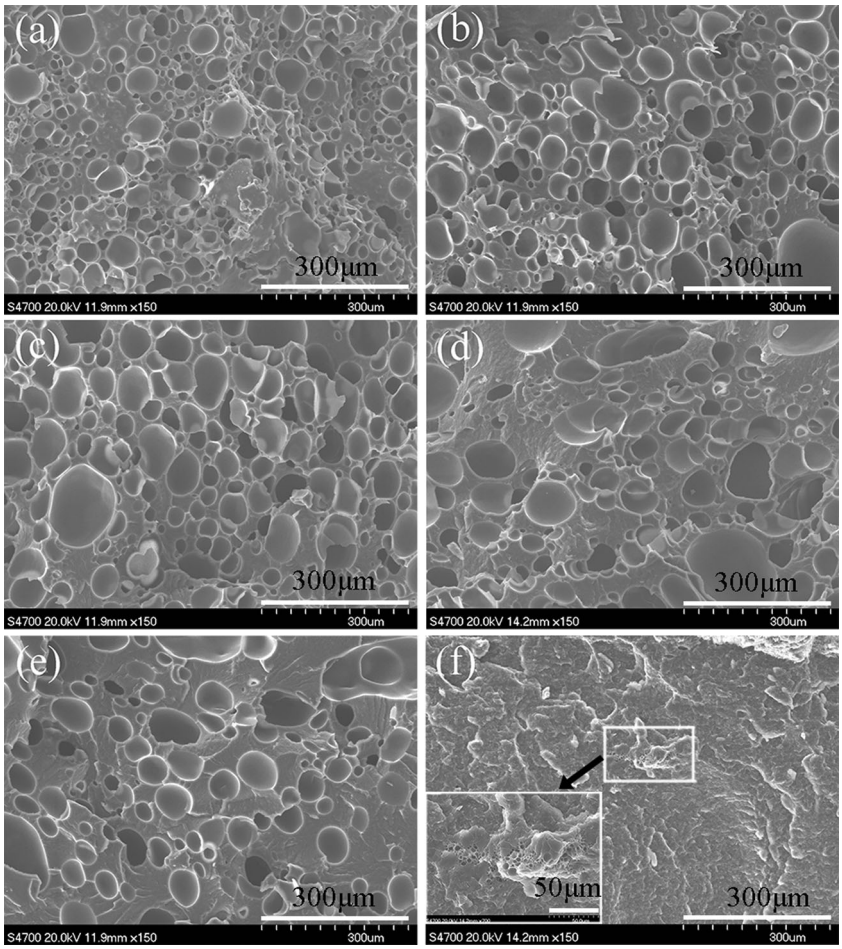

Fig. 22 SEM micrographs of foamed LCB-PPs with various processing times: (**a**) 0 min, (**b**) 5 min, (**c**) 10 min, (**d**) 20 min, (**e**) 40 min and (**f**) 60 min. All foams were obtained by saturating at 50 °C and 20 MPa for 10 h, then foaming at 190 °C

influenced even by the short-time processing in an internal mixer, whereas that of L-PP was unchanged. Since the molecular weight and the distribution was not affected by the processing history, the significant change of viscoelasticity was ascribed to 'shear modification', i.e., alignment of long branches to the backbone by the conformation change of molecules. It is also found that the relationship between the magnitude of shear modification and total processing history was linear on a logarithmic scale. G' and η^* at low frequency quickly decreased after shear; the G' curve moved closer to the terminal behavior curve and the shear-thinning became started at higher frequency with the prolonged processing time. The higher tan δ and smaller semicircle radius in Cole-Cole plot verified that disentanglement and alignment of side chains along back bone occurred during processing.

Further, the rheological properties of processed LCB-PP were recovered by vacuum-annealing to some extent, and this recovery process could be accelerated by raising the annealing temperature. It is interesting that the recovery process of rheological properties under high-pressure CO_2 atm was faster

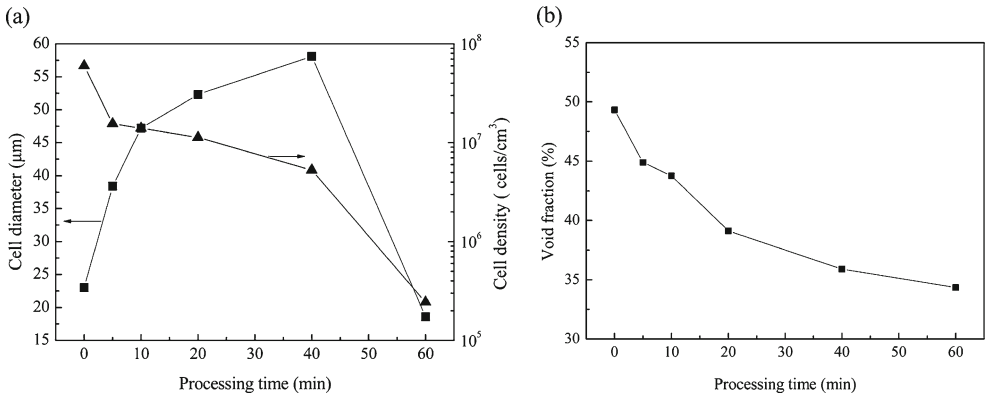

Fig. 23 Cell parameters for foamed LCB-PPs as a function of processing time, and all foams were obtained by saturating at 50 °C and 20 MPa for 10 h, then foaming at 190 °C: (**a**) cell diameter and cell density (**b**) void fraction

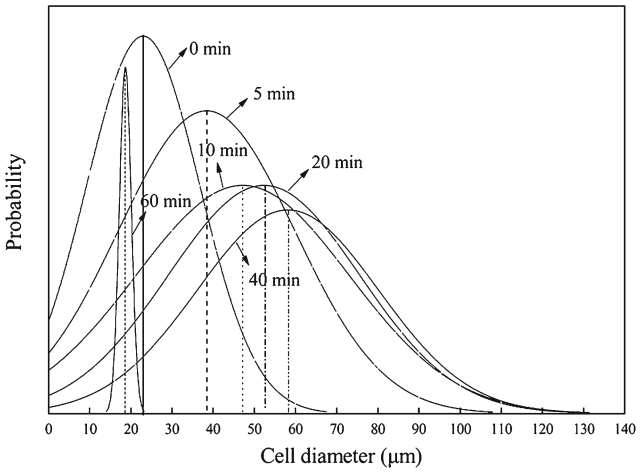

Fig. 24 Cell diameter distribution for foamed LCB-PPs and all foams were obtained by saturating at 50 °C and 20 MPa for 10 h, then foaming at 190 °C: (**a**) cell diameter and cell density (**b**) void fraction

than that under vacuum atmosphere, and higher CO_2 pressure resulted in higher recovery ratio. The superiority of high-pressure CO_2 saturation annealing was characterized by higher G' and η^* at low frequency, lower tan δ and bigger radius of Cole-Cole plot. This interesting phenomenon was attributed to the larger free volume for PP chain movement brought by CO_2, and the larger free volume shortened the annealing time required for long aligned branches to recover to their initial states.

Besides, the crystallization of LCB-PP was promoted and the peek temperature during crystallization was substantially increased by the applied processing history. At the same time, the changes in rheological properties after shear modification had great influence on the foamability of LCB-PP. Much larger cell size and lower cell density were found in the foamed LCB-PPs which had undergone more intense processing history.

Acknowledgments This work is supported by grant No. 2011BAD24B01 from the 12th National Five-Year Key Technology R&D Program of China and grant No. 51273019 from Natural Science Foundation of China.

References

1. Klempner D, Frisch KC (1991) Handbook of polymeric foams and foam technology. Hanser, Munich
2. Park CB, Cheung LK (1997) Polym Eng Sci 37:1–10
3. Lagendijk RP, Hogt AH, Buijtenhuijs A, Gotsis AD (2001) Polymer 42:10035–10043
4. Hingmann R (1994) J Rheol 38:573–588
5. Auhl D, Stange J, Münstedt H, Krause B, Voigt D, Lederer A, Lappan U, Lunkwitz K (2004) Macromol 37:9465–9472
6. Yamaguchi M, Todd DB, Gogos CG (2003) Adv Polym Technol 22:179–187
7. Yamaguchi M (2006) J Appl Polym Sci 102:1078–1083
8. Rokudai M (1979) J Appl Polym Sci 23:463–471
9. Rokudai M, Fujiki T (1979) J Appl Polym Sci 23:3295–3300
10. Rokudai M (1981) J Appl Polym Sci 26:1427–1429
11. Yamaguchi M, Takahashi M (2001) Polymer 42:8663–8670
12. Yamaguchi M, Gogos CG (2001) Adv Polym Technol 20:261–269
13. Hanson DE (1969) Polym Eng Sci 9:405–414
14. Teh JW, Rudin A, Schreiber HP (1985) J Appl Polym Sci 30:1345–1357
15. Baker WE, Rudin A, Schreiber HP, El-Kindi M (1993) Polym Eng Sci 33:377–382
16. Leblans PJR, Bastiaansen C (1989) Macromol 22:3312–3317
17. Breuer G, Schausberger A (2011) Rheol Acta 50:461–468
18. Zeng W, Liu J, Zhou J, Dong J, Yan S (2008) Chinese Sci Bull 53: 188–197
19. Su ZQ, Wang HY, Dong JY, Zhang XQ, Dong X, Zhao Y, Yu J, Han CC, Xu DF, Wang DJ (2007) Polymer 48:870–876
20. Wang XD, Zhang YX, Liu BG, Du ZJ, Li HQ (2008) Polym J 40: 450–454
21. Tian JH, Yu W, Zhou CX (2007) J Appl Polym Sci 104:3592–3600
22. Yu FY, Zhang HB, Liao RG, Zheng H, Yu W, Zhou CX (2009) Eur Polym J 45:2110–2118
23. Agarwal PK, Somani RH, Weng WQ, Mehta A, Yang L, Ran SF, Liu LZ, Hsiao BS (2003) Macromol 36:5226–5235
24. Kitade S, Asuka K, Akiba I, Sanada Y, Sakurai K, Masunaga H (2013) Polymer 54:246–257
25. Nam GJ, Yoo JH, Lee JW (2005) J Appl Polym Sci 96:1793–1800
26. Stange J, Münstedt H (2006) J Cell Plast 42:445–467
27. Stange J, Münstedt H (2006) J Rheol 50:907–923
28. Lin X, Rose FC, Ren DY, Wang KS, Coates P (2013) J Polym Res 20:122–133
29. Wen HY, Li H, Xu SY, Xiao SL, Li HF, Jiang SC, An LJ, Wu ZH (2012) J Polym Res 19:9801–9812
30. Wunderlich B (1973) Macromolecular physics, vol 1: Crystal structure morphology, defects. Academic, Waltham
31. Doi M, Edwards SF (1986) The theory of polymer dynamics. Clarendon, Oxford
32. Ruymbeke EV, Stephenne V, Daoust D, Godard P, Keunings R, Bailly C (2005) J Rheol 49:1503–1520
33. Franco CG, Srinivas S, Lohse DJ (2001) Macromol 34:3115–3117
34. Tian JH, Yu W, Zhou CX (2006) Polymer 47:7962–7969
35. Yamaguchi M, Wagner MH (2006) Polymer 47:3629–3635
36. Simha R, Somcynsky T (1969) Macromol 2:342–350
37. Li G, Wang J, Park CB, Simha R (2007) J Polym Sci Pol Phys 45: 2497–2508
38. Gupta AK, Purwar SN (1984) J Appl Polym Sci 29:1595–1609
39. Zhai WT, Wang HY, Yu J, Dong JY, He JS (2008) Polym Eng Sci 48:1312–1321